The American Journal of Pathology, Vol. 184, No. 5, May 2014

The American Journal of
PATHOLOGY
ajp.amjpathol.org

TUMORIGENESIS AND NEOPLASTIC PROGRESSION

Development of Hepatocellular Carcinoma in a Murine Model of Nonalcoholic Steatohepatitis Induced by Use of a High-Fat/Fructose Diet and Sedentary Lifestyle

Joanna K. Dowman,*† Laurence J. Hopkins,* Gary M. Reynolds,* Nikolaos Nikolaou,‡ Matthew J. Armstrong,*† Jean C. Shaw,* Diarmaid D. Houlihan,*† Patricia F. Lalor,* Jeremy W. Tomlinson,‡ Stefan G. Hübscher,§ and Philip N. Newsome*†

From the Department of NIHR Liver Biomedical Research Unit and Centre for Liver Research, and the Centre for Endocrinology, Diabetes and Metabolism,‡ University of Birmingham, Birmingham; and The Liver Unit† and the Department of Cellular Pathology,§ Queen Elizabeth Hospital Birmingham, Birmingham, United Kingdom*

Accepted for publication January 23, 2014.

Address correspondence to Laurence J. Hopkins, MBiochem, or Philip N. Newsome, Ph.D., M.D., Centre for Liver Research, Institute of Biomedical Research, School of Immunity and Infection, College of Medical and Dental Sciences, University of Birmingham, Edgbaston, Birmingham, United Kingdom B15 2TT. E-mail: ljh2g13@soton.ac.uk or p.n.newsome@bham.ac.uk.

Obesity is increasingly prevalent, strongly associated with nonalcoholic liver disease, and a risk factor for numerous cancers. Here, we describe the liver-related consequences of long-term diet-induced obesity. Mice were exposed to an extended obesity model comprising a diet high in *trans*-fats and fructose corn syrup concurrent with a sedentary lifestyle. Livers were assessed histologically using the nonalcoholic fatty liver disease (NAFLD) activity score (Kleiner system). Mice in the American Lifestyle-Induced Obesity Syndrome (ALIOS) model developed features of early nonalcoholic steatohepatitis at 6 months (mean NAFLD activity score = 2.4) and features of more advanced nonalcoholic steatohepatitis at 12 months, including liver inflammation and bridging fibrosis (mean NAFLD activity score = 5.0). Hepatic expression of lipid metabolism and insulin signaling genes were increased in ALIOS mice compared with normal chow-fed mice. Progressive activation of the mouse hepatic stem cell niche in response to ALIOS correlated with steatosis, fibrosis, and inflammation. Hepatocellular neoplasms were observed in 6 of 10 ALIOS mice after 12 months. Tumors displayed cytological atypia, absence of biliary epithelia, loss of reticulin, alteration of normal perivenular glutamine synthetase staining (absent or diffuse), and variable α-fetoprotein expression. Notably, perivascular tumor cells expressed hepatic stem cell markers. These studies indicate an adipogenic lifestyle alone is sufficient for the development of nonalcoholic steatohepatitis, hepatic stem cell activation, and hepatocarcinogenesis in wild-type mice. *(Am J Pathol 2014, 184: 1550–1561; http://dx.doi.org/10.1016/j.ajpath.2014.01.034)*

Nonalcoholic fatty liver disease (NAFLD) represents one of the commonest causes of liver disease in the Western world,[1] ranging in severity from steatosis to nonalcoholic steatohepatitis (NASH) and cirrhosis.[2] Although simple steatosis alone is relatively benign, the presence of steatohepatitis greatly increases the risk of progression to cirrhosis, with its concomitant risk of developing hepatocellular carcinoma (HCC)[3] and death.[4] Moreover, an evolving body of literature implicates obesity with the development of cancer,[5] including HCC.[6] Notably, although obesity is closely associated with NAFLD, not all patients are obese, and severe NASH may develop in nonobese patients,[2] indicating that the interaction of factors contributing to NAFLD pathogenesis is not fully understood. A need therefore exists for murine models that accurately reflect the causative factors underpinning clinical NASH to allow for the investigation of these factors that contribute to its development and progression to cancer.

Current rodent models of fatty liver disease rely on strains that carry spontaneous mutations (*ob/ob*[7], *db/db*[8]), genetic manipulations,[9] or formulated diets (methionine and choline deficient diet,[10] high-fat diet[11]), yet none of these models accurately reproduce the broad range of factors that contribute

Supported by the Wellcome Trust and the Biotechnology and Biological Sciences Research Council (BBSRC).
J.K.D. and L.J.H. contributed equally to this work.
J.W.T., S.G.H., and P.N.N. are joint senior authors.
Disclosures: None declared.

http://dx.doi.org/10.1016/j.ajpath.2014.01.034

to the histological spectrum of human NAFLD and its sequel. More recently, combinatorial use of diets with high proportions of fat, *trans*-fatty acids, oxidized lipoproteins,[12] or high-fructose drinking water[13] have resulted in patterns of liver injury closer to that observed in NASH, although aspects such as significant fibrogenesis and carcinogenesis are still lacking. Tetri et al[14] added a sedentary lifestyle to a diet rich in *trans*-fatty acids and high-fructose corn syrup for a 16-week period and found that mice developed glucose intolerance and hepatic steatosis and inflammation. Here, we report the effects of a prolonged version (12 months) of the American Lifestyle-Induced Obesity Syndrome (ALIOS) model that more accurately represents the extended pathogenesis of NASH seen clinically.

Material and Methods

Animal Treatment

Male C57BL/6 × 129 mice aged 6 to 8 weeks were housed in accordance with animal care protocols at the University of Birmingham, UK. Mice were maintained on a 12:12 hour light-dark schedule at 22°C, with up to four mice per cage. Individual animals were weighed weekly. ALIOS mice were fed a *trans*-fat custom diet (TD.06303; Harlan Teklad, Madison, WI) as previously reported.[14] Control mice were fed a standard chow diet with normal drinking water. Food and drink was provided *ad libitum* to all animals. A total of 20 mice received an ALIOS diet, of which 10 were sacrificed after 6 months and 10 at 12 months. Nineteen control mice received a normal chow (NC) diet for identical time periods with 10 sacrificed after 6 months and 9 sacrificed after 12 months. Ten mice were sacrificed aged 6 to 8 weeks for baseline measurements and histological assessments. Mice were sacrificed by cervical dislocation under terminal general anesthesia with the use of isoflurane.

Intraperitoneal Glucose Tolerance Tests

Glucose tolerance was measured by intraperitoneal glucose tolerance test 5 to 14 days before culling. Mice were fasted for 5 hours before baseline vein glucose testing from the tail vein by using a portable glucometer (Accuchek Aviva; Roche, Basel, Switzerland) at 15-, 30-, 60-, and 120-minute intervals after intraperitoneal injection of 1 mg/kg of a sterile 20% dextrose solution.

Triglyceride Quantification

Total hepatic triglyceride concentrations were measured with a triglyceride quantification kit (Biovision, Cambridge, UK) according to the manufacturer's instructions and read at OD 570 nm. Triglyceride concentration was calculated with a standard curve.

Pathology Assessments

Formalin-fixed liver sections were embedded in paraffin and sectioned (4 μm). Sections were stained with H&E to examine general morphology and with hematoxylin van Gieson for fibrosis. Slides were assessed by three authors (J.K.D., L.J.H., and G.M.R.), and a consensus interpretation was reached by review with an experienced liver pathologist (S.G.H.). Each section was allocated a NAFLD activity score (NAS) through blinded assessment according to the Kleiner scoring system. The Kleiner system generates a composite score that is based on the degree of steatosis (0 to 3), lobular inflammation (0 to 3), and hepatocyte ballooning (0 to 2), with a separate score for fibrosis (0 to 4).[15] Gross morphology and marker expression of hepatocellular neoplasms (summarized in Table 1) was assessed by S.G.H.

Immunohistochemistry

Immunohistochemistry (IHC) was performed as previously described[16] with the use of immPRESS secondary antibodies (Vector Labs, Burlingame, CA). IHC detection of 13 μg/mL α-fetoprotein (AFP; Dako, Glostrup, Denmark), 1:1000 α-smooth muscle action (Abcam, Cambridge, MA), 1 μg/mL β-catenin (Santa Cruz Biotech, Santa Cruz, CA), 5 μg/mL glutamine synthetase (GS; Millipore, Billerica, MA), 0.4 μg/mL Ki-67 (Millipore), 2 μg/mL pan-cytokeratin (pan-CK; Dako), 1 μg/mL Sox9 (Millipore),

Table 1 Characteristics of Hepatic Lesions in Mice Fed ALIOS Diet for 12 Months

Lesion number	Animal number	Lesion description	Size, mm	Reticulin fiber depletion	Glutamine synthetase*	β-cat†	Sox9†	AFP†	PI-FC
1	1	Microscopic	<1	+	2	−	−	−	1.61
2	2	Microscopic	<1	+	NA	−	+	−	2.05
3	3	Macroscopic	3	+	3	−	+	−	2.82
4	3	Macroscopic	3	+	2	+	−	−	17.58
5	3	Microscopic	<1	+	2	+	−	−	14.17
6	4	Microscopic	<1	−	2	+	−	−	7.89
7	4	Macroscopic	6	+	2	−	+	+	3.42
8	5	Macroscopic	5	+	1	−	+	+	6.8
9	6	Macroscopic	10	+	3	−	+	+	6.96

*Normal perivenular pattern is indicated by 1, diffuse up-regulation by 2, and absence by 3.
†Presence (+) or absence (−).
NA, not applicable; PI-FC, proliferation index (percentage of Ki-67$^+$) fold change in tumor versus background liver.

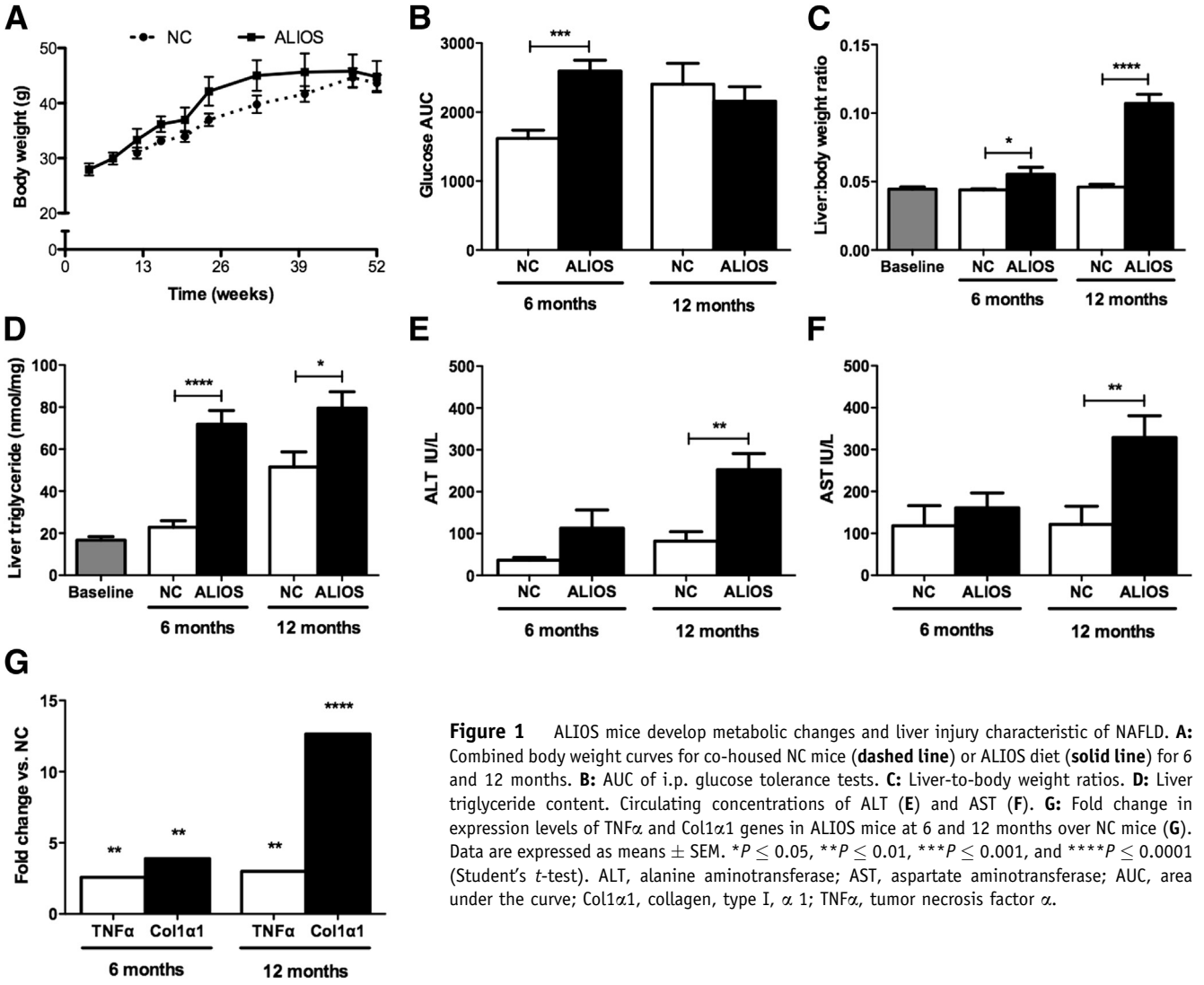

Figure 1 ALIOS mice develop metabolic changes and liver injury characteristic of NAFLD. **A:** Combined body weight curves for co-housed NC mice (**dashed line**) or ALIOS diet (**solid line**) for 6 and 12 months. **B:** AUC of i.p. glucose tolerance tests. **C:** Liver-to-body weight ratios. **D:** Liver triglyceride content. Circulating concentrations of ALT (**E**) and AST (**F**). **G:** Fold change in expression levels of TNFα and Col1α1 genes in ALIOS mice at 6 and 12 months over NC mice (**G**). Data are expressed as means ± SEM. $*P \leq 0.05$, $**P \leq 0.01$, $***P \leq 0.001$, and $****P \leq 0.0001$ (Student's *t*-test). ALT, alanine aminotransferase; AST, aspartate aminotransferase; AUC, area under the curve; Col1α1, collagen, type I, α 1; TNFα, tumor necrosis factor α.

1:1000 ubiquitin (Dako), and 40 μg/mL CK18 (Abcam) was performed. Staining was quantified by assessing five random nonoverlapping views per sample centered on portal tracts at ×200 magnification with the use of ImageJ software version 10.2 (*http://rsbweb.nih.gov/ij*). Pan-CK staining was quantified by calculating the mean stained area with the use of ImageJ analysis. Sox9 IHC was quantified by counting the mean number of positive parenchymal cells observed in five ×200 fields, and Ki-67 by the mean number of cells in five ×400 fields.

RNA Analysis

Fresh liver tissue was stored in RNALater (Sigma, St. Louis, MO) at 4°C overnight and then at −80°C. RNA isolation was performed with the Qiagen RNEasy MiniKit (Qiagen, Valencia, CA) according to standard protocol, and RNA concentration was measured by spectrophotometry (NanoDrop Technologies, Labtech International, East Sussex, UK). Taqman 20× gene expression singleplex real-time quantitative PCR assays (Applied Biosystems, Carlsbad, CA) were used to measure mRNA expression. Results were normalized to the RNA, 18S ribosomal 5 gene. Fold changes were calculated with transformation (fold increase $= 2^{\Delta Ct}$).

Statistical Analysis

Glucose tolerance was analyzed by one-way analysis of variance and Student's *t*-test comparison of the means ± SEM area under the curve of the different groups. Comparisons of grouped data were performed with Student's *t*-test or Welch's *t*-test when variances were significantly different. Statistical analysis of real-time quantitative PCR data was performed with ΔCt values.

Results

ALIOS Mice Develop Metabolic Changes and Liver Injury Characteristic of NAFLD

Weight gain was greater in ALIOS mice than in NC mice after 6 months, although weights converged by 12 months

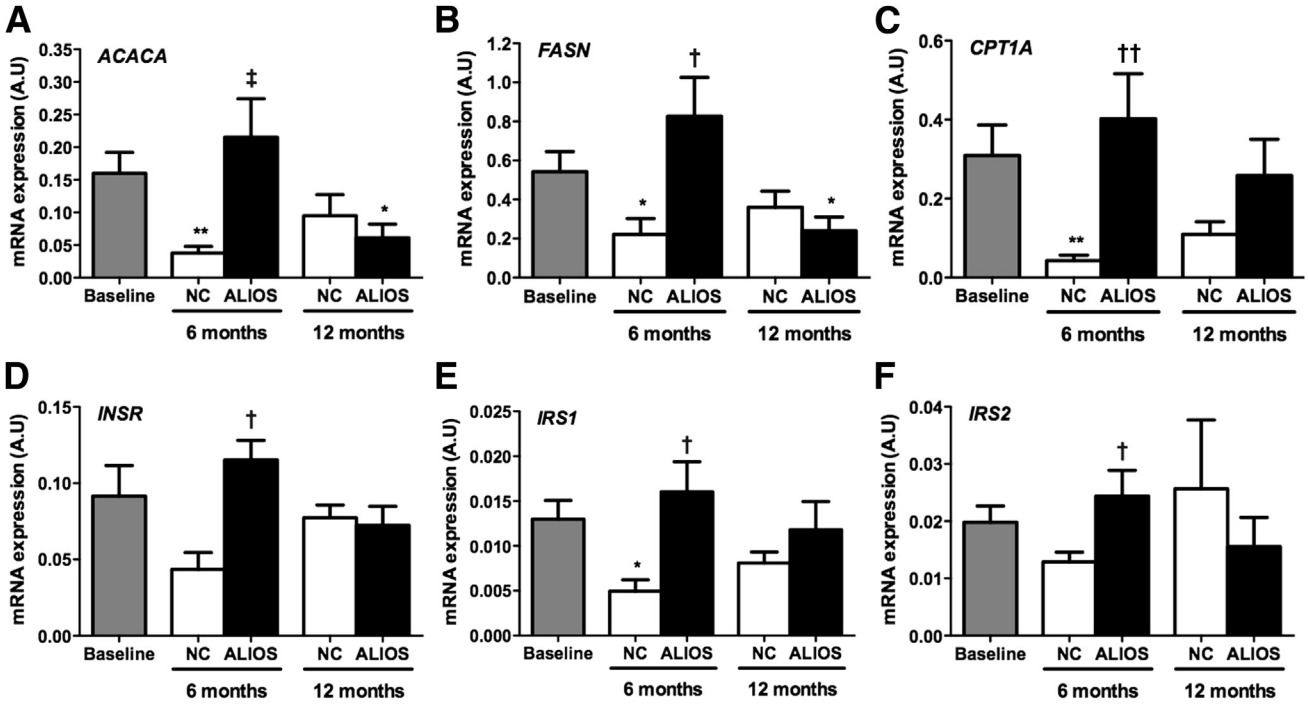

Figure 2 Increased lipid turnover in ALIOS mice at 6 months. Hepatic mRNA expression of *ACACA* (**A**), *FASN* (**B**), *CPT1A* (**C**), *INSR* (**D**), *IRS1* (**E**), and *IRS2* (**F**) measured by real-time PCR in mice fed normal chow (black bars) or ALIOS diet (gray bars) for either 6 or 12 months. Additional comparisons are made against baseline liver samples (white bars). Data are expressed as means ± SEM in arbitrary units (A.U.); n = 8 to 10 animals in each group. $^{*}P < 0.05$, $^{**}P < 0.01$ versus baseline; $^{\dagger}P < 0.05$, $^{\dagger\dagger}P < 0.01$ versus normal chow at same time point. *ACACA*, acetyl CoA carboxylase; *CPT1A*, carnitine palmitoyltransferase; *FASN*, fatty acid synthase; *INSR*, insulin receptor; *IRS1*, insulin receptor substrate 1; *IRS2*, insulin receptor substrate 2.

(Figure 1A). Glucose tolerance was reduced in ALIOS mice compared with NC mice at 6 months, but this difference was not maintained at 12 months, by which time NC mice were similar (Figure 1B). Liver-to-body weight ratios were higher in ALIOS mice than in chow-fed mice at both 6 and 12 months (Figure 1C) with greater levels of hepatic triglycerides measured in livers of ALIOS mice than in NC mice (Figure 1D). ALIOS mice had elevated levels of serum alanine aminotransferase (Figure 1E) and aspartate aminotransferase (Figure 1F) at 12 months compared with NC mice. Expression of the tumor necrosis factor gene and collagen, type I, α 1 gene was increased in the ALIOS cohort at 6 and 12 months compared with chow-fed mice at the same time points in keeping with induction of inflammatory and fibrogenic processes in response to the ALIOS diet (Figure 1G). Activated stellate cells shown by α-smooth muscle actin IHC were clearly increased in number in the ALIOS cohort at 12 months but were infrequent or absent at 6 months and in the other cohorts (Supplemental Figure S1).

Increased Expression of Lipid Metabolism and Insulin Signaling Genes in ALIOS Mice

Expression of acetyl-CoA carboxylase 1 and fatty acid synthase, genes coding for key regulators of lipogenesis, was increased in ALIOS mice at 6 and 12 months compared with NC mice (Figure 2, A and B). Expression of carnitine palmitoyltransferase 1 gene, a rate-limiting enzyme necessary for β-oxidation of long chain fatty acids, was increased in ALIOS mice at 6 months compared with NC mice but not at 12 months (Figure 2C). Although the activity of these gene products was mainly regulated at the post-transcriptional levels, these data represented increased lipid turnover (increased lipogenesis and β-oxidation) in livers of ALIOS mice. Expressions of insulin receptor gene, insulin receptor substrate 1 gene, and insulin receptor substrate 2 gene were increased in ALIOS mice at 6 months compared with NC mice but not at 12 months (Figure 2, D–F). Up-regulation of these genes at 6 months that was lost by 12 months could indicate a failure to compensate for dietary stresses in ALIOS mice by 12 months.

ALIOS Mice Develop Histological Features of NASH

Baseline (8-week-old) mice displayed no evidence of liver injury or steatosis (Figure 3A), whereas NC mice developed mild steatosis of mixed droplet size with a predominantly perivenular distribution at 12 months (Figure 3B). In ALIOS mice steatosis was more severe, more diffuse, and progressed with time. Moderate macrovesicular steatosis with a predominantly periportal distribution was typically seen at 6 months (Figure 3C). This pattern of steatosis persisted for ALIOS mice at 12 months by which time microvesicular steatosis was also prominent in perivenular

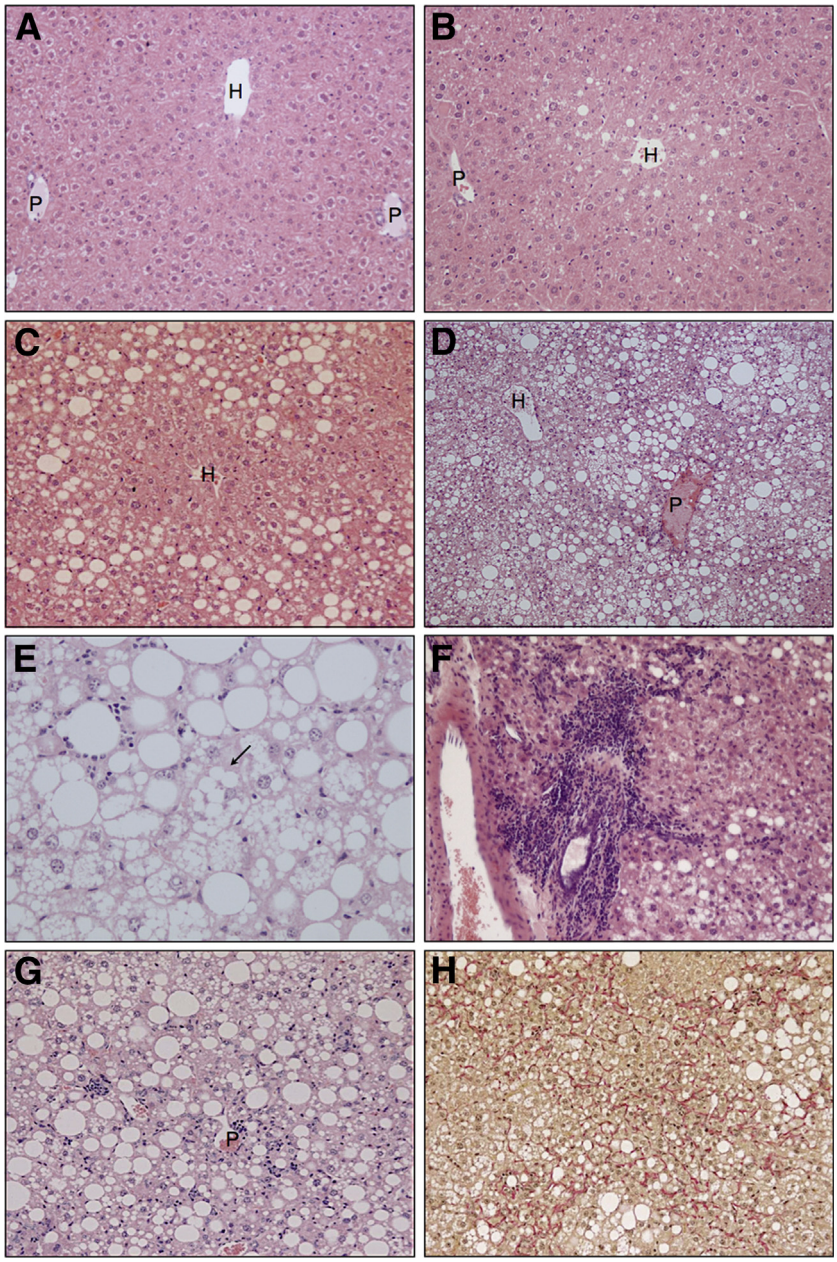

Figure 3 ALIOS mice develop histological features of NASH. **A:** Baseline mouse (8-week-old) shows no evidence of steatosis. **B:** Normal chow mouse at 12 months shows very mild perivenular steatosis. **C:** Moderate macrovesicular steatosis with a predominantly periportal distribution in an ALIOS mouse at 6 months. **D:** Severe panlobular steatosis in an ALIOS mouse at 12 months. Macrovesicular steatosis still has a mainly periportal distribution. Microvesicular steatosis is more prominent in perivenular regions. **E:** Mixed large and small droplet fatty change in an ALIOS mouse at 12 months. The **arrow** indicates a cell thought to have possible ballooning. However, no definite Mallory-Denk bodies were found by immunostaining for ubiquitin and K18 (data not shown). Portal inflammation (**F**) and lobular inflammation (**G**) in an ALIOS mouse at 12 months. **H:** Pericellular and bridging fibrosis in an ALIOS mouse at 12 months (**H**). H&E stain (**A**–**G**); van Gieson stain (**H**). H, hepatic vein; P, portal tract.

regions (Figure 3D). Steatosis was mild or moderate after 6 months of ALIOS diet (Figure 3C) and severe in 9 of 10 mice at 12 months (Figure 3D). The presence of ballooned hepatocytes and Mallory-Denk bodies was characteristic features of NASH.[17] Distinction of ballooned hepatocytes from the frequently extensive microvesicular steatosis made assessment of this histological feature difficult. Although occasional cells with a ballooned appearance were initially thought to be present in H&E-stained sections from ALIOS mice at 6 and 12 months (Figure 3E), no definite Mallory-Denk bodies were identified by immunostaining for ubiquitin or K18 (data not shown). For all animals the ballooning component of the NAS was thus scored as 0. In addition, no increase was found in the expression of sonic hedgehog in mice on the ALIOS diet (Supplemental Figure S2). ALIOS diet induced lobular inflammation in 7 of 10 ALIOS-fed mice at 6 months that was not observed in any chow-fed mice at this time point. At 12 months lobular inflammation was present in 9 of 10 of the ALIOS cohort and in 2 of 9 of the chow-fed mice. Lobular inflammatory cells comprised a mixed population of lymphocytes and neutrophils (Figure 3F), with periportal inflammatory infiltrates observed in 4 of 10 ALIOS mice at 12 months (Figure 3G). Fibrosis was observed histologically in 8 of 10 ALIOS mice and in 1 of 9 chow-fed mice at 12 months. In all cases, fibrosis had a perisinusoidal pattern similar to that observed in human NASH. Among ALIOS mice at 12 months, fibrosis severity ranged from mild periportal through to bridging fibrosis. The latter was characterized by the presence of diffuse dissection of the parenchyma by

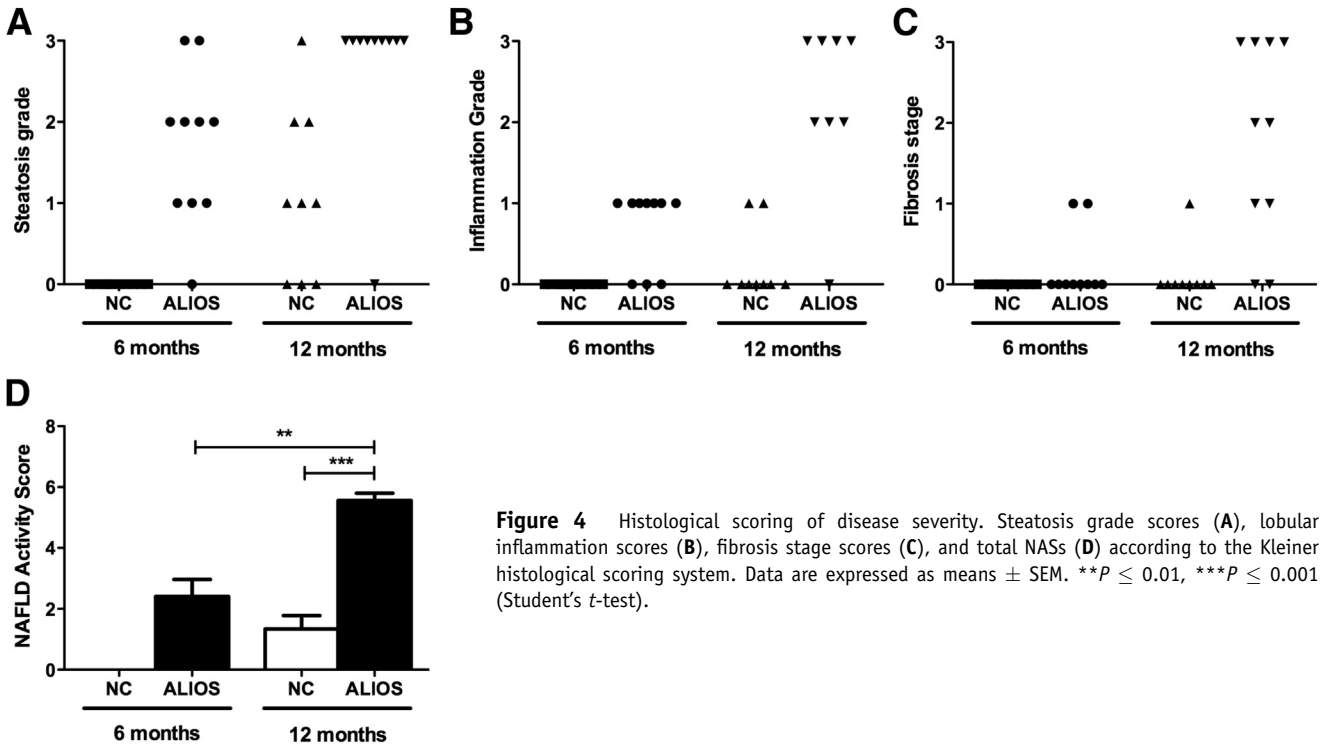

Figure 4 Histological scoring of disease severity. Steatosis grade scores (**A**), lobular inflammation scores (**B**), fibrosis stage scores (**C**), and total NASs (**D**) according to the Kleiner histological scoring system. Data are expressed as means ± SEM. $^{**}P \leq 0.01$, $^{***}P \leq 0.001$ (Student's *t*-test).

delicate strands of perisinusoidal collagen without the development of broader fibrous septa (Figure 3H). The single NC mouse with fibrosis at 12 months only had mild periportal fibrosis. Cirrhosis was not observed in any mice.

The use of the Kleiner histological system (NAS) indicated significantly increased severity of steatosis grade ($P = 0.003$) (Figure 4A), lobular inflammation ($P < 0.0001$) (Figure 4B), and fibrosis stage ($P = 0.001$) (Figure 4C) in ALIOS mice compared with NC mice at 12 months. At 6 months, none of the 10 NC mice scored for any components of NAS, whereas ALIOS-fed mice had a mean NAS of 2.4 ± 0.6. By 12 months, NC mice had a mean NAS of 1.3 ± 0.4 and ALIOS-fed mice a mean NAS of 5.0 ± 0.6 ($P < 0.001$) (Figure 4D).

Hepatic Stem Cell Activation in ALIOS Mice Correlates with Histological Features of NASH

Pan-CK IHC has been previously used to identify hepatic progenitor (oval cells) and ductular reactive cells in rodents.[18] More recently Sox9, a nuclear transcription factor, has been reported as a marker of hepatic progenitor cells,[19] allowing a more specific population of stem/progenitor cells to be identified by IHC than with pan-CK. Pan-CK and Sox9 expression in livers of baseline mice had a similar pattern to those of NC mice at 12 months, whereby pan-CK expression was found to be largely restricted to the biliary epithelium (Figure 5A). Sox9 immunostaining was likewise positive within the biliary epithelium (Figure 5B). In contrast, by 12 months ALIOS mice had greatly increased numbers of pan-CK$^+$ and Sox9$^+$ cells observed throughout the parenchyma in addition to cells located within the biliary epithelium seen in chow-fed animals (Figure 5, C and D). This observation was confirmed by quantification of the percentage area covered by pan-CK$^+$ cells and the number of observed Sox9$^+$ cells per area (Figure 5, E and F). Increased accumulation of pan-CK$^+$ and Sox9$^+$ cells was closely associated with severe steatosis (score = 3), lobular inflammation (score ≥ 2), and fibrosis severity (score ≥ 2) (Figure 5, G and H).

ALIOS Mice Develop Hepatocellular Neoplasms That Contain Perivascular Sox9$^+$ Tumor Cells

A total of nine lesions (five macroscopic and four microscopic) were observed in 6 of 10 ALIOS mice (60%) (Table 1). Macroscopically visible nodules (diameter > 3 mm) developed in 4 of 10 ALIOS mice (40%) at 12 months (Figure 6A), of which two nodules were found in one mouse. No macroscopic nodules or microscopic foci of atypical hepatocytes were seen in any NC mice.

All of the lesions identified macroscopically and microscopically were well circumscribed and well differentiated. Macroscopic lesions were associated with compression of adjacent nonlesional tissue, but no invasion of blood vessels, portal tract stroma, or surrounding liver tissue was seen. Histological examination showed lesions composed of hepatocytes with low-grade cytological atypia in the form of mild nuclear pleomorphism, a slightly increased nuclear-to-cytoplasmic ratio, and occasional mitoses. Microscopic foci (<1 mm diameter) composed of atypical hepatocytes with a similar appearance were present in a further two

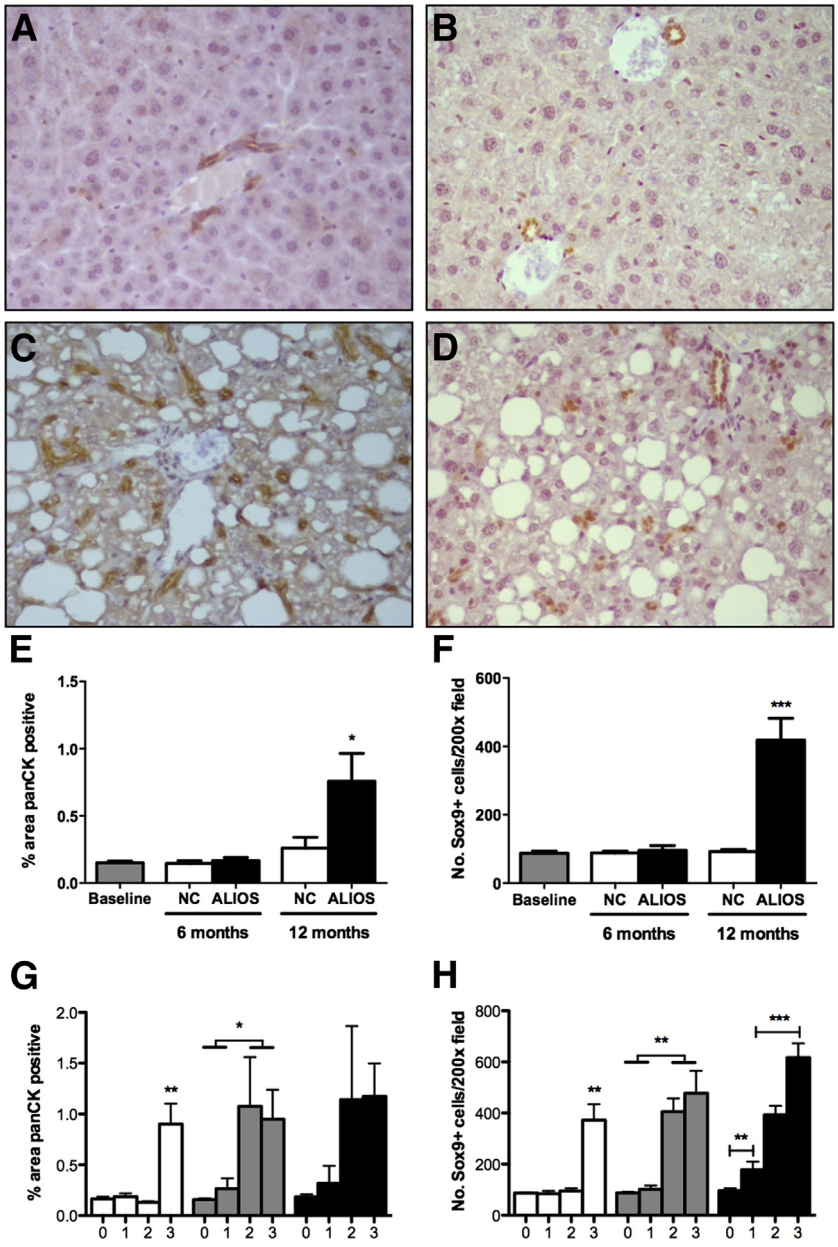

Figure 5 Hepatic stem cell activation in ALIOS mice correlates with histological features of NASH. Representative examples of pan-CK (**A**) and Sox9 (**B**) IHC of livers from NC mice at 12 months. Representative examples of pan-CK (**C**) and Sox9 (**D**) IHC of livers from ALIOS mice at 12 months. Mean percentage area covered by pan-CK$^+$ cells (**E**) and average number of Sox9$^+$ cells (**F**) per $\times$200 field, in liver sections from baseline, NC, and ALIOS mice. Correlation between histological scores and mean percentage covered by pan-CK$^+$ cells (**G**) and average number for Sox9$^+$ cells (**H**) per $\times$200 field. Data are expressed as means $\pm$ SEM. $^*P \leq 0.05$, $^{**}P \leq 0.01$, and $^{***}P \leq 0.001$ (analysis of variance with Bonferonni's correction).

ALIOS-fed mice (Figure 6B). In the absence of evidence of invasion to confirm a definite diagnosis of malignancy we attempted to further characterize these lesions by using additional markers (Table 1) that have been shown to be altered in previous studies of rodent models[20,21] and/or human HCC.[22,23]

AFP is expressed by hepatoblasts during liver development but is absent in rodent and adult liver.[24] Detection of circulating AFP is routinely used clinically in the screening and early detection of HCC in high-risk patients.[25] We observed a small proportion of AFP$^+$ tumor cells in three of five macroscopic lesions in ALIOS mice (Figure 6C) but an absence of AFP$^+$ tumor cells in microscopic lesions and background liver of all mice. Loss of the normal reticulin fiber pattern is a characteristic feature of human HCC, although reticulin fibers are sometimes retained in well-differentiated neoplasms. Reticulin staining was difficult to assess because it was somewhat patchy in nonlesional liver tissue. However, a clear reduction in the number of reticulin fibers present could be observed in all (five) macroscopically visible nodules from ALIOS-fed mice (Figure 6D). Reticulin fibers also appeared to be reduced, to a lesser extent, in three of four microscopic foci. Up-regulation of GS expression is a feature that has been used to distinguish well-differentiated HCC from premalignant lesions in the human liver.[26] In nonlesional liver, we observed a perivenular distribution of GS, similar to the pattern of expression seen in normal human liver (Figure 6E). Diffuse staining for GS was present in three of the four atypical microscopic foci seen in ALIOS-fed mice, similar to the pattern that has been described in human HCC (Figure 6F). Interestingly, three of five macroscopic nodules appeared to have a reduced expression of GS, with loss of the

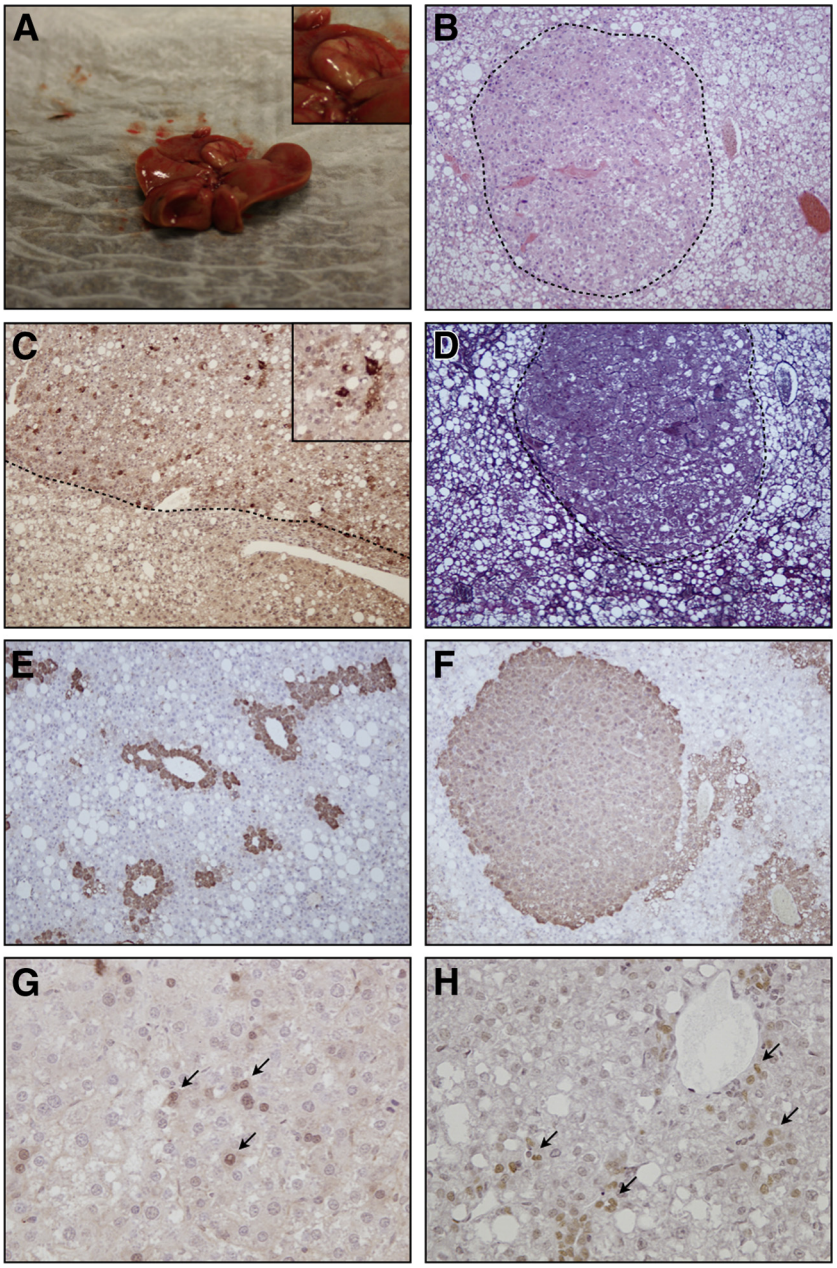

Figure 6 ALIOS mice develop HCC that contains perivascular Sox9^{+} tumor cells. **A:** Representative example of macroscopic hepatocellular lesion from ALIOS mouse at 12 months. **B:** Representative example of microscopic hepatocellular lesion (**dotted line**) from NC mouse at 12 months by H&E staining. **C:** AFP IHC of macroscopic hepatocellular lesion (above **dotted line**) shows the presence of AFP^{+} tumor cells. **Inset** show a higher magnification image of AFP^{+} tumor cells. **D:** Representative example of absent reticulin staining in a macroscopic hepatocellular lesion (**dashed line**) from ALIOS mouse at 12 months. There is compression of the normal reticulin framework in surrounding nonlesional tissue. Examples of GS IHC of liver from baseline mice (**E**) and microscopic lesion from ALIOS mouse (**F**) at 12 months. **G:** Example of nuclear accumulation of β-catenin (**arrows**) in cells of hepatocellular lesion from ALIOS mouse at 12 months. **H:** Example of perivascular Sox9^{+} tumor cells (**arrows**) of hepatocellular lesion from ALIOS mouse at 12 months.

normal perivenular pattern of staining (Supplemental Figure S3). Aberrant nuclear accumulation of β-catenin was indicative of tumorigenesis and was associated with increased tumor progression and a worse prognosis.[27] A small proportion (<5%) of tumor cells in three lesions (one macroscopic and two microscopic) displayed nuclear accumulation of β-catenin (Figure 6G).

Sox9, a marker of murine hepatic stem cell (mHpSC) and primitive stem cells of the biliary and intestinal epithelium,[28] was observed in the nuclei of neoplastic hepatocytes in five nodules (four macroscopic and one microscopic). These appeared to be preferentially located in a perivascular distribution, but otherwise they had a similar morphology to surrounding tumor cells, without obvious evidence of biliary differentiation (Figure 6H).

With the use of Ki-67 IHC (Table 1), we observed increased proportions of proliferating hepatocytic tumor cells compared with the proportion of proliferating hepatocytes in background liver (16.0% ± 7.3% versus 3.0% ± 1.6%; $P = 0.001$). Moreover, turnover was higher in nodules that contained tumor cells with nuclear accumulation of β-catenin, fold change in proliferation index over background (13.2 ± 4.9 versus 3.9 ± 2.4; $P = 0.005$).

Discussion

In this study we demonstrate that mice exposed to the ALIOS lifestyle for an extended period of 12 months develop a broad spectrum of NAFLD-related histological

Table 2 Comparison of Human NASH and the Murine ALIOS Model

Characteristics	Human NASH	Murine ALIOS
Clinical features		
Cause	Multifactorial (diet/environment/genetics)	Diet alone
Body weight	Significant association with obesity and central adiposity	Weight gain (then subsequent loss with severe disease burden)
Hepatomegaly	Clinical sign (not present in all cases)	Increased liver-to-body weight ratios at 6 and 12 months
Glucose intolerance (diabetes)	Significant association with insulin resistance and type 2 diabetes; reciprocal risk factors	Observed at 6 months
Blood markers	Elevated ALT and AST, but can have significant disease with normal LFTs	Elevated ALT and AST at 12 months
Hepatic tumorigenesis	Significant risk of HCC development in NASH cirrhosis (versus normal population)	Hepatocellular lesions observed in 50% of animals at 12 months
Histopathology		
Steatosis distribution and pattern	Early stages = perivenular macrovesicular Later stages = panacinar with mixture of macrovesicular and microvesicular steatosis	Periportal macrovesicular steatosis at 6 months Periportal macrovesicular and perivenular microvesicular steatosis at 12 months
Steatosis severity	Variable; in end-stage cirrhosis steatosis may be absent	Moderate at 6 months Severe at 12 months
Inflammation	Portal and lobular inflammation	Portal and lobular inflammation
Hepatocyte ballooning	Diagnostic of definite NASH*	Not identified
Fibrosis	Perisinusoidal ± periportal progressing to bridging fibrosis; broad septa and nodules (cirrhosis) in late-stage disease	Perisinusoidal ± periportal progressing to bridging pericellular fibrosis at 12 months; no broad septa or cirrhosis at 12 months
Hepatic stem/progenitor cells	Activation of hepatic progenitor cells commonly seen in periportal and periseptal ductular reactions	Periportal expansion of hepatic progenitors into surrounding parenchyma observed as single cells and ductules

*According to American Gastroenterological Association guidelines in 2012.
ALT, alanine aminotransferase; AST, aspartate aminotransferase; LFT, liver function test.

changes, including severe steatosis, lobular inflammation, fibrosis, and hepatocellular neoplasia. We also demonstrate a marked expansion of mouse HpSC and their close association with neoplastic foci in a clinically relevant model of NASH.

The distribution of steatosis observed in ALIOS mice was of an initial predominantly macrovesicular periportal steatosis with relative sparing of acinar zones 2 and 3. With time and disease progression, increasing microvesicular steatosis that extended into the centrilobular region was observed. A similar zonal variation in the distribution of microvesicular and macrovesicular steatosis in ALIOS mice was also observed in the study by Tetri et al.[14] Of note, the extensive microvesicular steatosis observed with the ALIOS diet may also reflect more progressive disease, because a recent large study found that this feature correlated with more severe histological changes in human NAFLD liver biopsies.[29] Quantification of liver triglyceride confirmed these histological findings, with significantly greater triglyceride in the ALIOS livers than in control livers at 6 months, although by 12 months this difference was reduced by a significant increase in the control group. This observation is again consistent with the predisposition of aging mice to the development of a metabolic phenotype.[30]

Although developed for assessing the severity of NAFLD in human liver tissue, the NAS has also been used in other murine studies. In the present study NAS was significantly higher in the ALIOS cohort at both 6 and 12 months. By 12 months, although several of the control mice had developed some features of NAFLD (ie, mainly steatosis), NAS scores in the ALIOS group were significantly higher. The assessment of hepatocyte ballooning in humans is used diagnostically, yet our understanding of the causative contribution of hepatocyte ballooning in the pathogenesis of NASH remains unclear. Despite applying three staining techniques routinely used for the assessment of ballooning (H&E, ubiquitin, and K18) we were unable to observe hepatocyte ballooning in response to ALIOS. Our observations appear to be similar to those of Tetri et al[14] who observed in their 16-week model of ALIOS some cytoplasm alterations and clumping, suggestive of ballooning, and possible Mallory hyaline in zone 3. However, only H&E staining was reported in this study, and additional IHC was not used to confirm the presence of Mallory-Denk bodies. We were unable to discern whether the lack of ballooning in our study was due to intrinsic variation between rodent and human liver injury or the extended duration of the ALIOS diet to 6 and 12 months. Severe steatosis, bridging fibrosis, and hepatic stem cell activation were observed in the

ALIOS model at 12 months. However, differences between murine and human histopathology was observed in the pattern and distribution of steatosis, fibrosis, and stem cell proliferation (Table 2).

Histological fibrosis was observed in only two of the ALIOS mice and no control animals at 6 months, and in both cases it was in a periportal (stage 1c) distribution. However, collagen, type I, α 1 mRNA expression was 4.2-fold higher in the ALIOS mice at this time point, providing additional evidence of an early fibrotic response. By 12 months, fibrosis was observed in only one of the controls (10%) but in eight of the ALIOS mice (80%), four of which showed bridging fibrosis. The >10-fold increase in collagen, type I, α 1 expression in the ALIOS cohort at this time point was consistent with these findings.

Currently used rodent models of chronic hepatic injury, HpSC activation, and hepatocarcinogenesis rely on the use of toxic agents[31] or genetic manipulations[32] that fail to replicate the complex pathogenesis of NAFLD. This study provides the first detailed characterization of a clinically relevant murine model of metabolic liver injury and provides new data on the spatiotemporal association between NAFLD, mHpSC activation, and the development of hepatic dysplasia/cancer. In human disease, loss of mature biliary epithelial cells and hepatocytes, as occurs in chronic biliary diseases and metabolic liver disease, respectively, results in a marked accumulation of hHpSC.[33–35] Activation of the mHpSC niche has been extensively studied in a range of murine liver injury models, including genetic,[36] diet,[37] bile duct ligation,[38] and alcohol,[39] but activation in nontoxic diet models with the use of wild-type mice has previously not been reported. Here, we demonstrate activation of the mHpSC niche in response to the ALIOS model of chronic metabolic liver injury with the use of pan-CK and Sox9 IHC. The number of mHpSC observed increased with duration and severity of liver injury and correlated with increased fibrosis, inflammation, and steatosis but were largely absent from NC mice. Our findings support the observation of a close association between hHpSC activation and histological features of chronic liver injury in humans.[40]

The finding of hepatocellular neoplasms in 6 of 10 ALIOS mice is of significant concern, given the high population consumption of both high-fructose corn syrup and *trans*-fatty acids. HCC is a well-recognized complication of advanced NASH in humans and is also increasingly recognized to occur in noncirrhotic NASH.[41] Previous rodent models of HCC have described the development of a spectrum of similar focal hepatocellular lesions,[20,21] which have been variously classified as preneoplastic foci, dysplastic foci, adenoma, and benign hepatoma, as well as HCC. Similar problems have been encountered with the classification of precursor lesions and early HCC in human livers.[22,23]

The extent to which the murine lesions are comparable with hepatocellular neoplasms in human liver has not been fully established. In an attempt to address this problem, we performed detailed characterization, using many of the markers used to diagnose early HCC in human livers. This characterization revealed many features consistent with that of early human HCC, including the loss of biliary structures, disruption or loss of reticulin fibers, aberrant expression of GS and AFP, and nuclear accumulation of β-catenin. These changes were accompanied by various degrees of cytological atypia that are also recognized as a feature of human HCC, establishing this as a novel model for the study of HCC development on the background of NASH.

Sox9 is a marker of endodermal stem cells in liver, pancreas, biliary tree, and intestine,[28] and its expression is associated with progression of a number of tumors.[42–44] Although studies have suggested a causal link between hHpSC and HCC development,[36] a direct link between $Sox9^+$ hHpSC and HCC development and progression has yet to be described. In this study we report for the first time the presence of small foci of perivascular $Sox9^+$ tumor cells in murine HCC, which also notably express higher levels of Ki-67 indicative of higher proliferative rates. Increasing evidence suggests that small populations of tumor cells possess significantly greater abilities for self-renewal and tumor initiation than other cells of the tumor bulk.[45] These cells also frequently express stem cell-related markers and are found in perivascular locations,[46] suggesting that the presence of perivascular $Sox9^+$ tumor cells may represent a cancer stem cell niche within HCC tumors of ALIOS mice. It is possible that these $Sox9^+$ cells represent a form of transitional cell between a stem cell and a neoplastic hepatocyte. We are unable to determine the cell of origin for the tumors observed in ALIOS mice or to assess the contribution of $Sox9^+$ tumor cells to the development and progression of HCC, although their close spatial association requires further research. Further work with the use of cell fate tracking experiments specifically labeling mHpSC in a relevant injury model will aid in determining the origin of $Sox9^+$ HCC tumor cells but was not possible in this study.

This study found that the environmental factors are sufficient in causing the full spectrum of NAFLD but did not determine the relative importance of individual components through the use of interventions or assessed the potential contribution of genetic variables. Despite the length of this model, further studies that use targeted interventions or genetic manipulation will have value in aiding the identification of patients at highest risk of progression and interventions or pharmacologic agents that have efficacy in the treatment of NAFLD.

In conclusion, we report the development of a clinically relevant murine model of NASH which replicates many of the features seen in human disease, as well as demonstrating activation of the hepatic stem cell niche in response to dietary and lifestyle changes. This study demonstrates that, in the absence of toxins or genetic variation, high-fat/fructose diet and sedentary lifestyle are sufficient for the induction of NASH, stem cell mediated-regeneration, and hepatocarcinogenesis in wild-type mice.

Acknowledgments

J.K.D., conception and design, acquisition and assembly of data and data analyses, interpretation, figures, manuscript writing and editing; L.J.H., acquisition and assembly of data and data analyses, interpretation, figures, tables, initial manuscript preparation and editing; G.M.R., N.N., M.J.A., D.D.H., and J.C.S., acquisition and assembly of data and data analyses, interpretation, manuscript editing; P.F.L., data analyses, interpretation, manuscript writing and editing; J.W.T., conception and design, data analyses and interpretation, manuscript writing and editing, final approval of manuscript; S.G.H., data acquisition and analyses (particularly histological assessments), interpretation, manuscript writing and editing, final approval of manuscript; P.N.N., conception and design, assembly of data, data analyses and interpretation, manuscript writing and editing, final approval of manuscript and financial support.

Supplemental Data

Supplemental material for this article can be found at *http://dx.doi.org/10.1016/j.ajpath.2014.01.034*.

References

1. Armstrong MJ, Houlihan DD, Bentham L, Shaw JC, Cramb R, Olliff S, Gill PS, Neuberger JM, Lilford RJ, Newsome PN: Presence and severity of non-alcoholic fatty liver disease in a large prospective primary care cohort. J Hepatol 2012, 56:234–240
2. Angulo P: Nonalcoholic fatty liver disease. N Engl J Med 2002, 346: 1221–1231
3. Ascha MS, Hanouneh IA, Lopez R, Tamimi TA, Feldstein AF, Zein NN: The incidence and risk factors of hepatocellular carcinoma in patients with nonalcoholic steatohepatitis. Hepatology 2010, 51:1972–1978
4. Adams LA, Lymp JF, St Sauver J, Sanderson SO, Lindor KD, Feldstein A, Angulo P: The natural history of nonalcoholic fatty liver disease: a population-based cohort study. Gastroenterology 2005, 129: 113–121
5. Khandekar MJ, Cohen P, Spiegelman BM: Molecular mechanisms of cancer development in obesity. Nat Rev Cancer 2011, 11:886–895
6. Yoshimoto S, Loo TM, Atarashi K, Kanda H, Sato S, Oyadomari S, Iwakura Y, Oshima K, Morita H, Hattori M, Honda K, Ishikawa Y, Hara E, Ohtani N: Obesity-induced gut microbial metabolite promotes liver cancer through senescence secretome. Nature 2013, 499:97–101
7. Bijl N, Sokolovic M, Vrins C, Langeveld M, Moerland PD, Ottenhoff R, van Roomen CP, Claessen N, Boot RG, Aten J, Groen AK, Aerts JM, van Eijk M: Modulation of glycosphingolipid metabolism significantly improves hepatic insulin sensitivity and reverses hepatic steatosis in mice. Hepatology 2009, 50:1431–1441
8. Witek RP, Stone WC, Karaca FG, Syn WK, Pereira TA, Agboola KM, Omenetti A, Jung Y, Teaberry V, Choi SS, Guy CD, Pollard J, Charlton P, Diehl AM: Pan-caspase inhibitor VX-166 reduces fibrosis in an animal model of nonalcoholic steatohepatitis. Hepatology 2009, 50:1421–1430
9. Horie Y, Suzuki A, Kataoka E, Sasaki T, Hamada K, Sasaki J, Mizuno K, Hasegawa G, Kishimoto H, Iizuka M, Naito M, Enomoto K, Watanabe S, Mak TW, Nakano T: Hepatocyte-specific Pten deficiency results in steatohepatitis and hepatocellular carcinomas. J Clin Invest 2004, 113:1774–1783
10. Leclercq IA, Farrell GC, Field J, Bell DR, Gonzalez FJ, Robertson GR: CYP2E1 and CYP4A as microsomal catalysts of lipid peroxides in murine nonalcoholic steatohepatitis. J Clin Invest 2000, 105:1067–1075
11. Lo L, McLennan SV, Williams PF, Bonner J, Chowdhury S, McCaughan GW, Gorrell MD, Yue DK, Twigg SM: Diabetes is a progression factor for hepatic fibrosis in a high fat fed mouse obesity model of non-alcoholic steatohepatitis. J Hepatol 2011, 55:435–444
12. Yimin, Furumaki H, Matsuoka S, Sakurai T, Kohanawa M, Zhao S, Kuge Y, Tamaki N, Chiba H: A novel murine model for non-alcoholic steatohepatitis developed by combination of a high-fat diet and oxidized low-density lipoprotein. Lab Invest 2012, 92:265–281
13. Kohli R, Kirby M, Xanthakos SA, Softic S, Feldstein AE, Saxena V, Tang PH, Miles L, Miles MV, Balistreri WF, Woods SC, Seeley RJ: High-fructose, medium chain trans fat diet induces liver fibrosis and elevates plasma coenzyme Q9 in a novel murine model of obesity and nonalcoholic steatohepatitis. Hepatology 2010, 52:934–944
14. Tetri LH, Basaranoglu M, Brunt EM, Yerian LM, Neuschwander-Tetri BA: Severe NAFLD with hepatic necroinflammatory changes in mice fed trans fats and a high-fructose corn syrup equivalent. Am J Physiol Gastrointest Liver Physiol 2008, 295:G987–G995
15. Kleiner DE, Brunt EM, Van Natta M, Behling C, Contos MJ, Cummings OW, Ferrell LD, Liu YC, Torbenson MS, Unalp-Arida A, Yeh M, McCullough AJ, Sanyal AJ; Nonalcoholic Steatohepatitis Clinical Research Network: Design and validation of a histological scoring system for nonalcoholic fatty liver disease. Hepatology 2005, 41:1313–1321
16. Shetty S, Weston CJ, Oo YH, Westerlund N, Stamataki Z, Youster J, Hubscher SG, Salmi M, Jalkanen S, Lalor PF, Adams DH: Common lymphatic endothelial and vascular endothelial receptor-1 mediates the transmigration of regulatory T cells across human hepatic sinusoidal endothelium. J Immunol 2011, 186:4147–4155
17. Brunt EM: Nonalcoholic steatohepatitis: definition and pathology. Semin Liver Dis 2001, 21:3–16
18. Germain L, Goyette R, Marceau N: Differential cytokeratin and alpha-fetoprotein expression in morphologically distinct epithelial cells emerging at the early stage of rat hepatocarcinogenesis. Cancer Res 1985, 45:673–681
19. Dorrell C, Erker L, Schug J, Kopp JL, Canaday PS, Fox AJ, Smirnova O, Duncan AW, Finegold MJ, Sander M, Kaestner KH, Grompe M: Prospective isolation of a bipotential clonogenic liver progenitor cell in adult mice. Genes Dev 2011, 25:1193–1203
20. Weber A, Boger R, Vick B, Urbanik T, Haybaeck J, Zoller S, Teufel A, Krammer PH, Opferman JT, Galle PR, Schuchmann M, Heikenwalder M, Schulze-Bergkamen H: Hepatocyte-specific deletion of the antiapoptotic protein myeloid cell leukemia-1 triggers proliferation and hepatocarcinogenesis in mice. Hepatology 2010, 51: 1226–1236
21. Nejak-Bowen KN, Thompson MD, Singh S, Bowen WC Jr, Dar MJ, Khillan J, Dai C, Monga SP: Accelerated liver regeneration and hepatocarcinogenesis in mice overexpressing serine-45 mutant beta-catenin. Hepatology 2010, 51:1603–1613
22. Goodman ZD, Terraciano L, Wee A: Tumours and tumour-like lesions of the liver. Edited by Burt AD, Portmann BC, Ferrell LD. MacSween's Pathology of the Liver. 6th ed. London, Churchill Livingstone Elsevier, 2012, pp 761–851
23. Park YN: Update on precursor and early lesions of hepatocellular carcinomas. Arch Pathol Lab Med 2011, 135:704–715
24. Schmelzer E, Wauthier E, Reid LM: The phenotypes of pluripotent human hepatic progenitors. Stem Cells 2006, 24:1852–1858
25. Sato Y, Nakata K, Kato Y, Shima M, Ishii N, Koji T, Taketa K, Endo Y, Nagataki S: Early recognition of hepatocellular carcinoma based on altered profiles of alpha-fetoprotein. N Engl J Med 1993, 328:1802–1806
26. Di Tommaso L, Franchi G, Park YN, Fiamengo B, Destro A, Morenghi E, Montorsi M, Torzilli G, Tommasini M, Terracciano L, Tornillo L, Vecchione R, Roncalli M: Diagnostic value of HSP70, glypican 3, and glutamine synthetase in hepatocellular nodules in cirrhosis. Hepatology 2007, 45:725–734

27. Nhieu JT, Renard CA, Wei Y, Cherqui D, Zafrani ES, Buendia MA: Nuclear accumulation of mutated beta-catenin in hepatocellular carcinoma is associated with increased cell proliferation. Am J Pathol 1999, 155:703−710
28. Furuyama K, Kawaguchi Y, Akiyama H, Horiguchi M, Kodama S, Kuhara T, Hosokawa S, Elbahrawy A, Soeda T, Koizumi M, Masui T, Kawaguchi M, Takaori K, Doi R, Nishi E, Kakinoki R, Deng JM, Behringer RR, Nakamura T, Uemoto S: Continuous cell supply from a Sox9-expressing progenitor zone in adult liver, exocrine pancreas and intestine. Nat Genet 2011, 43:34−41
29. Tandra S, Yeh MM, Brunt EM, Vuppalanchi R, Cummings OW, Unalp-Arida A, Wilson LA, Chalasani N; NASH Clinical Research Network (NASH CRN): Presence and significance of microvesicular steatosis in nonalcoholic fatty liver disease. J Hepatol 2011, 55: 654−659
30. Anstee QM, Goldin RD: Mouse models in non-alcoholic fatty liver disease and steatohepatitis research. Int J Exp Pathol 2006, 87:1−16
31. Wang B, Hsu SH, Frankel W, Ghoshal K, Jacob ST: Stat3-mediated activation of microRNA-23a suppresses gluconeogenesis in hepatocellular carcinoma by down-regulating glucose-6-phosphatase and peroxisome proliferator-activated receptor gamma, coactivator 1 alpha. Hepatology 2012, 56:186−197
32. Nakanishi Y, Tsuneyama K, Nomoto K, Fujimoto M, Salunga TL, Nakajima T, Miwa S, Murai Y, Hayashi S, Kato I, Hiraga K, Hsu DK, Liu FT, Takano Y: Nonalcoholic steatohepatitis and hepatocellular carcinoma in galectin-3 knockout mice. Hepatol Res 2008, 38:1241−1251
33. Richardson MM, Jonsson JR, Powell EE, Brunt EM, Neuschwander-Tetri BA, Bhathal PS, Dixon JB, Weltman MD, Tilg H, Moschen AR, Purdie DM, Demetris AJ, Clouston AD: Progressive fibrosis in nonalcoholic steatohepatitis: association with altered regeneration and a ductular reaction. Gastroenterology 2007, 133:80−90
34. Roskams TA, Theise ND, Balabaud C, Bhagat G, Bhathal PS, Bioulac-Sage P, Brunt EM, Crawford JM, Crosby HA, Desmet V, Finegold MJ, Geller SA, Gouw AS, Hytiroglou P, Knisely AS, Kojiro M, Lefkowitch JH, Nakanuma Y, Olynyk JK, Park YN, Portmann B, Saxena R, Scheuer PJ, Strain AJ, Thung SN, Wanless IR, West AB: Nomenclature of the finer branches of the biliary tree: canals, ductules, and ductular reactions in human livers. Hepatology 2004, 39:1739−1745
35. Lowes KN, Brennan BA, Yeoh GC, Olynyk JK: Oval cell numbers in human chronic liver diseases are directly related to disease severity. Am J Pathol 1999, 154:537−541
36. Yang S, Koteish A, Lin H, Huang J, Roskams T, Dawson V, Diehl AM: Oval cells compensate for damage and replicative senescence of mature hepatocytes in mice with fatty liver disease. Hepatology 2004, 39:403−411
37. Jelnes P, Santoni-Rugiu E, Rasmussen M, Friis SL, Nielsen JH, Tygstrup N, Bisgaard HC: Remarkable heterogeneity displayed by oval cells in rat and mouse models of stem cell-mediated liver regeneration. Hepatology 2007, 45:1462−1470
38. Sackett SD, Li Z, Hurtt R, Gao Y, Wells RG, Brondell K, Kaestner KH, Greenbaum LE: Foxl1 is a marker of bipotential hepatic progenitor cells in mice. Hepatology 2009, 49:920−929
39. Jung Y, Brown KD, Witek RP, Omenetti A, Yang L, Vandongen M, Milton RJ, Hines IN, Rippe RA, Spahr L, Rubbia-Brandt L, Diehl AM: Accumulation of hedgehog-responsive progenitors parallels alcoholic liver disease severity in mice and humans. Gastroenterology 2008, 134:1532−1543
40. Roskams T, Yang SQ, Koteish A, Durnez A, DeVos R, Huang X, Achten R, Verslype C, Diehl AM: Oxidative stress and oval cell accumulation in mice and humans with alcoholic and nonalcoholic fatty liver disease. Am J Pathol 2003, 163:1301−1311
41. Paradis V, Zalinski S, Chelbi E, Guedj N, Degos F, Vilgrain V, Bedossa P, Belghiti J: Hepatocellular carcinomas in patients with metabolic syndrome often develop without significant liver fibrosis: a pathological analysis. Hepatology 2009, 49:851−859
42. Zhou CH, Ye LP, Ye SX, Li Y, Zhang XY, Xu XY, Gong LY: Clinical significance of SOX9 in human non-small cell lung cancer progression and overall patient survival. J Exp Clin Cancer Res 2012, 31:18
43. Prevot PP, Simion A, Grimont A, Colletti M, Khalaileh A, Van den Steen G, Sempoux C, Xu X, Roelants V, Hald J, Bertrand L, Heimberg H, Konieczny SF, Dor Y, Lemaigre FP, Jacquemin P: Role of the ductal transcription factors HNF6 and Sox9 in pancreatic acinar-to-ductal metaplasia. Gut 2012, 61:1723−1732
44. Sashikawa Kimura M, Mutoh H, Sugano K: SOX9 is expressed in normal stomach, intestinal metaplasia, and gastric carcinoma in humans. J Gastroenterol 2011, 46:1292−1299
45. Borovski T, De Sousa E melo F, Vermeulen L, Medema JP: Cancer stem cell niche: the place to be. Cancer Res 2011, 71:634−639
46. Calabrese C, Poppleton H, Kocak M, Hogg TL, Fuller C, Hamner B, Oh EY, Gaber MW, Finklestein D, Allen M, Frank A, Bayazitov IT, Zakharenko SS, Gajjar A, Davidoff A, Gilbertson RJ: A perivascular niche for brain tumor stem cells. Cancer Cell 2007, 11:69−82